East European Journal of Physics. 4. 240-249 (2024)
DOI:10.26565/2312-4334-2024-4-24 ISSN 2312-4334

CHANGES IN THE STRUCTURE AND PROPERTIES OF SILICON DURING YTTERBIUM DOPING: THE RESULTS OF A COMPREHENSIVE ANALYSIS

Khodjakbar S. Daliev, Sharifa B. Utamuradova, Jonibek J. Khamdamov*, Mansur B. Bekmuratov, Shahriyor B. Norkulov, Ulugbek M. Yuldoshev
Institute of Semiconductor Physics and Microelectronics at the National University of Uzbekistan, 20 Yangi Almazar st., Tashkent, 100057, Uzbekistan
**Corresponding Author e-mail: jonibek.uzmu@gmail.com*
Received September 13, 2024; revised October 20, 2024; accepted October 20, 2024

In this work, a comprehensive study of the structural, chemical and electrophysical properties of monocrystalline silicon (Si) doped with ytterbium (Yb) has been carried out. The alloying was carried out by thermal diffusion at a temperature of 1473 K in high vacuum conditions followed by rapid cooling. Atomic force microscopy (AFM), infrared Fourier spectroscopy (FTIR), deep level spectroscopy (DLTS) and Raman spectroscopy (RAMAN) were used to analyze the samples obtained. AFM images of the surface of the doped samples demonstrated significant changes in topography. The RMS surface roughness increased from less than 10 nm to 60-80 nm, and the maximum height of the irregularities reached 325 nm. These changes are explained by the formation of nanostructures caused by the uneven distribution of ytterbium atoms in the silicon crystal lattice, as well as the occurrence of internal stresses. "IR-Fourier spectroscopy showed a significant decrease in the concentration of optically active oxygen (N_O^{opt}) by 30-40% after doping. This effect is associated with the interaction of ytterbium atoms with silicon and a change in the chemical composition of the material. The RAMAN spectra revealed the formation of new phases and nanocrystallites in the doped samples. Peak shifts and changes in their intensity were detected, indicating a rearrangement of the crystal lattice caused by the introduction of ytterbium. It was calculated that the diffusion coefficient of ytterbium in silicon is 1.9×10^{-15} cm^2/s, which indicates a slow diffusion process characteristic of rare earth metals. Electrical measurements carried out on the MDS-structures showed a shift in the volt-farad characteristics towards positive bias voltages, which is associated with a decrease in the density of surface states at the Si-SiO_2 interface and the appearance of deep levels with an ionization energy of E_c-0.32 eV.
Keywords: *Monocrystalline silicon, Ytterbium doping, Atomic force microscopy, Raman spectroscopy, Surface roughness, Nanostructures, Electrical properties, MDS-structures, Si-SiO_2 interface*
PACS: 68.37.Ps, 33.20.Fb

INTRODUCTION

The development and improvement of materials for semiconductor electronics remain key directions in modern science and technology [1-5]. Silicon, which is the main material for semiconductor devices, has unique properties [2-8]. However, in order to further improve it, it is necessary to use various alloying methods. The introduction of atoms of other elements into the silicon crystal lattice makes it possible to significantly change its properties and open up new possibilities for creating highly efficient electronic devices.

Special attention is given to rare earth elements (REE) such as yttrium, dysprosium, and ytterbium, which can significantly affect the structural and physical properties of silicon. Doping silicon with ytterbium (Yb) is a particularly interesting area of research since this element possesses unique physicochemical properties, including low chemical activity and a divalent state, making it a promising candidate for the creation of new semiconductor materials. As a rare earth element, ytterbium is not well-studied in terms of its effect on the crystal structure of silicon. However, preliminary studies indicate that doping silicon with ytterbium may lead to significant changes in its microstructure, including the formation of defects, nanocrystals, and changes in the material's phase composition. These structural transformations play an important role in determining the physical properties of silicon, such as conductivity and resistance to radiation exposure.

To study these structural changes in detail, atomic force microscopy (AFM) was used in this research. AFM allows for the visualization of material surfaces at the nanoscale, making it possible to detect changes in topography and surface structure caused by ytterbium doping [9-10]. The obtained data showed that doping leads to significant surface irregularities in silicon, with a maximum height of up to 325 nm, indicating a complex microstructure formed due to the uneven distribution of ytterbium atoms in the crystal lattice. In addition to AFM data, the study used methods of infrared Fourier spectroscopy (FTIR) and Raman spectroscopy (RAMAN) to study phase changes and the distribution of impurities in silicon. These methods revealed a reduction in the concentration of optically active oxygen, the formation of new phases and nanocrystals, as well as the evaluation of internal stress in the crystal lattice.

Thus, this study is aimed at deepening knowledge about structural changes in ytterbium-doped silicon and their effect on the physico-chemical properties of the material. The use of AFM in combination with other spectroscopic methods provides a more complete understanding of the processes occurring in doped silicon, which can become the basis for further developments in the field of semiconductor electronics and optoelectronics [11-18].

Cite as: Kh.S. Daliev, Sh.B. Utamuradova, J.J. Khamdamov, M.B. Bekmuratov, Sh.B. Norkulov, U.M. Yuldoshev. East Eur. J. Phys. 4, 240 (2024), https://doi.org/10.26565/2312-4334-2024-4-24

MATERIALS AND METHODS

For the experiment, samples of monocrystalline silicon with an initial resistivity ranging from 2.5 to 10 Om·cm were selected. The samples underwent thorough chemical cleaning to remove contaminants and oxide layers from the surface. This was done using an acid-peroxide wash, followed by treatment in hydrofluoric acid (HF), which ensured the complete removal of oxides and provided a clean silicon surface for subsequent doping.

After cleaning, high-purity ytterbium (Yb) films (99.999%) were deposited on the silicon surface. The deposition was carried out by vacuum sputtering under high vacuum conditions (10^{-6} Torr) using an oil-free vacuum system, which ensured uniform distribution of ytterbium atoms on the silicon surface. The doping process was performed using the thermal diffusion method. Prepared n-Si samples were placed in vacuum-sealed quartz ampoules and subjected to diffusion annealing at 1473 K (1200°C) for 15 hours. The samples were then rapidly cooled to prevent the formation of large defects and to ensure the uniform distribution of ytterbium within the silicon crystal lattice. Rapid cooling also promoted the creation of internal stresses in the samples, which could affect the formation of nanocrystals and other structural changes. After thermal diffusion, the surface layer of the samples, approximately 2 μm thick, was removed for the investigation of the doped deeper layers. This was achieved using mechanical treatment and chemical etching, allowing the study of structural changes at various depth levels.

To study the surface topography of the samples after ytterbium doping, atomic force microscopy (AFM) was used. AFM provides nanometer-resolution imaging, making it an indispensable tool for analyzing structural changes in materials. The studies were conducted on a Nanaview-2000 series microscope, which ensured high-precision measurements. Measurements were performed in several modes, including contact and semi-contact modes, to obtain information about the height of surface irregularities, the distribution of structural defects, and phase heterogeneities. 3D surface maps obtained using AFM allowed the evaluation of the maximum heights of structural elements (up to 325 nm) and revealed the distribution characteristics of ytterbium in silicon.

For chemical composition analysis and the study of molecular vibrations in the doped samples, Infrared Fourier spectroscopy (FTIR) was employed. FTIR absorption spectra were obtained using the FSM 2201 infrared Fourier spectrometer, operating in the range from 380 to 7800 cm^{-1}. The FTIR method allowed the determination of the concentration of optically active oxygen (NO_{opt}) in silicon and the identification of ytterbium's effect on the chemical composition and structure of the samples. Spectral analysis showed that ytterbium doping reduced the concentration of NO_{opt} by 30-40%, depending on the concentration of the introduced impurities.

Raman spectroscopy was used to investigate structural changes and phase composition. Raman spectra were obtained using an Ocean Insight Raman spectrometer with laser radiation at a wavelength of 780 nm. Raman spectroscopy revealed the formation of nanocrystals in the ytterbium-doped silicon samples. Three bands were identified, corresponding to Si–Si, Si–Yb, and Yb–Yb bond vibrations. The intensity and position of these bands varied depending on the composition and thermal treatment conditions. The internal stress in the crystallites, which could reach up to 3 GPa, was also studied.

For processing and analyzing the obtained spectra, FSpec software was used for FTIR spectroscopy, and OriginPro was used for Raman data analysis. Data processing included baseline subtraction, spectrum normalization, and the calculation of crystallite sizes from Raman peaks. The analysis results allowed for the evaluation of ytterbium's influence on the structural properties of silicon and the identification of key doping features, such as defect formation, changes in phase composition, and internal stress in the crystals.

RESULTS AND DISCUSSION

Analysis of AFM images revealed significant changes in the surface topography of silicon after ytterbium doping (Fig. 1). Prior to doping, the silicon surface was relatively smooth, with minimal irregularities and defects. The root-mean-square (RMS) roughness of the control sample was less than 10 nm, and the maximum height of the irregularities did not exceed 78.1 nm (Fig. 1a). After ytterbium doping, a sharp increase in the maximum height of surface irregularities up to 325 nm was observed in the near-surface layer, representing a substantial change (Fig. 1c). Doping with rare earth metals, such as ytterbium, induces local changes in the crystalline structure of silicon. Ytterbium has a larger atomic radius compared to silicon, which leads to distortions in the crystal lattice and the formation of internal stresses. These stresses can cause the formation of microdefects and recrystallization at grain boundaries, contributing to the increase in surface roughness.

According to Gibbs' theory, surface energy depends on crystallographic orientation and the presence of impurities. The introduction of ytterbium atoms increases the free surface energy, driving the system to reduce this energy by forming structures with higher roughness. The RMS roughness of the ytterbium-doped silicon surface is 60-80 nm in the near-surface layer, which is significantly higher than that of the control sample. This increase in roughness is associated with the formation of nanostructures or clusters of ytterbium on the surface.

To assess the change in surface energy, Gibbs' expression for surface energy can be used:

$$\gamma = \frac{dW}{dA}, \tag{1}$$

where γ is the surface energy, W is the work to change the surface, A is the surface area.

As the surface roughness increases, the surface area A also increases, which leads to an increase in the surface energy γ. An increase in surface energy may also explain the tendency of the material to form larger structures on the surface.

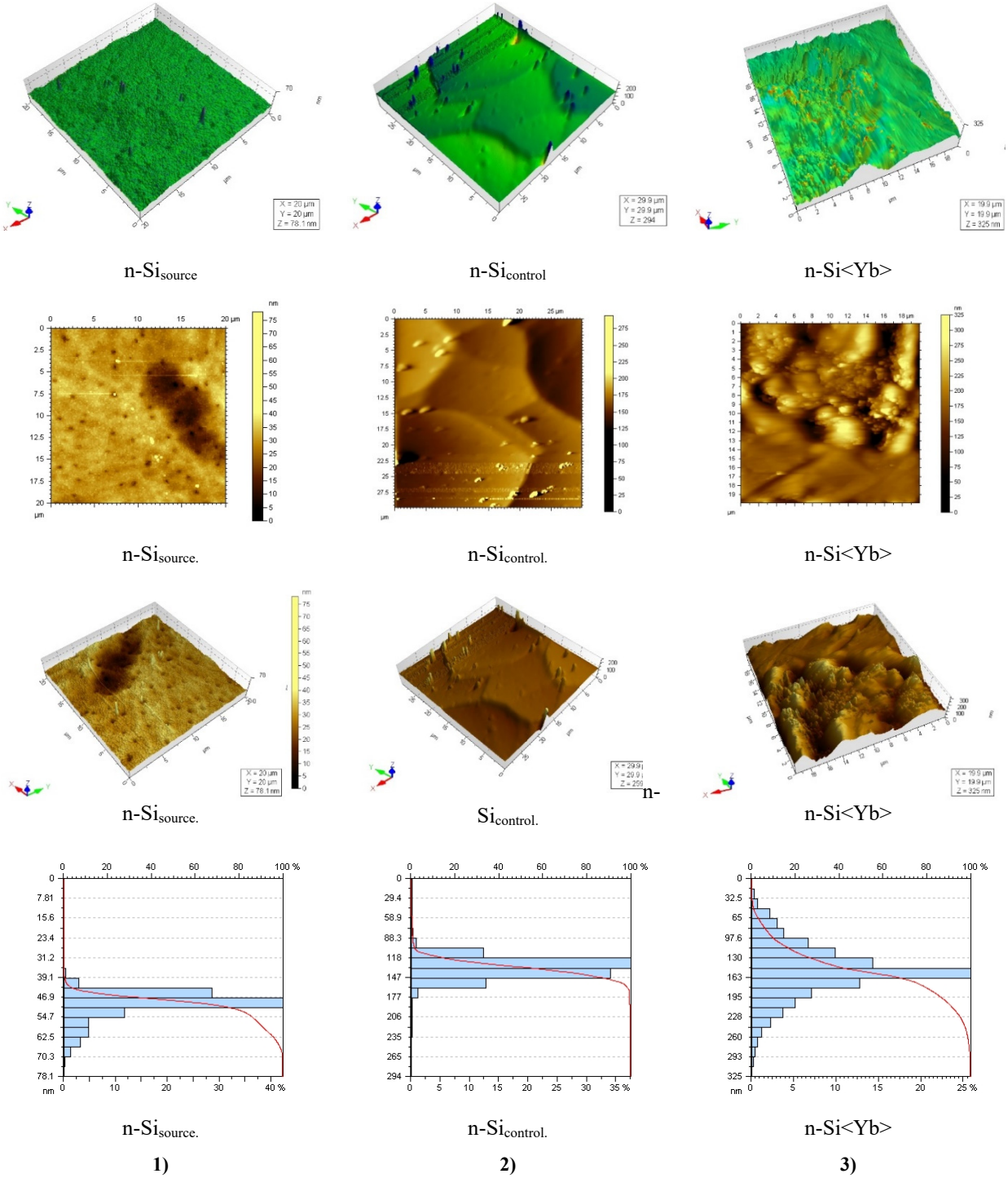

Figure 1. Atomic Force Microscopy (AFM) Images:
1) n-Si original sample; 2) n-Si control sample; 3) n-Si doped with ytterbium, with a 2 μm layer removed by grinding after doping

Phase analysis shows the presence of inhomogeneities, which are associated with the uneven distribution of ytterbium in the silicon structure. In the near-surface layer, the phases are distributed unevenly, indicating ytterbium agglomeration and the formation of new phases on the silicon surface.

Let's consider the changes in phase composition through the analysis of phase thermodynamic stability. Doping can cause the formation of ytterbium-containing phases, such as $YbSi_2$, which stabilize under certain conditions. The calculation of the change in Gibbs free energy during the formation of such phases can be expressed by:

$$\Delta G = \Delta H - T\Delta S, \quad (2)$$

where ΔG is the change in Gibbs free energy, ΔH is the enthalpy of formation, ΔS is the change in entropy, T is the temperature.

If G < 0, the phase is stable and can form on the surface. In this case, during high-temperature annealing and subsequent rapid cooling, the formation of thermodynamically stable ytterbium phases is likely, which explains the phase inhomogeneities on the surface.

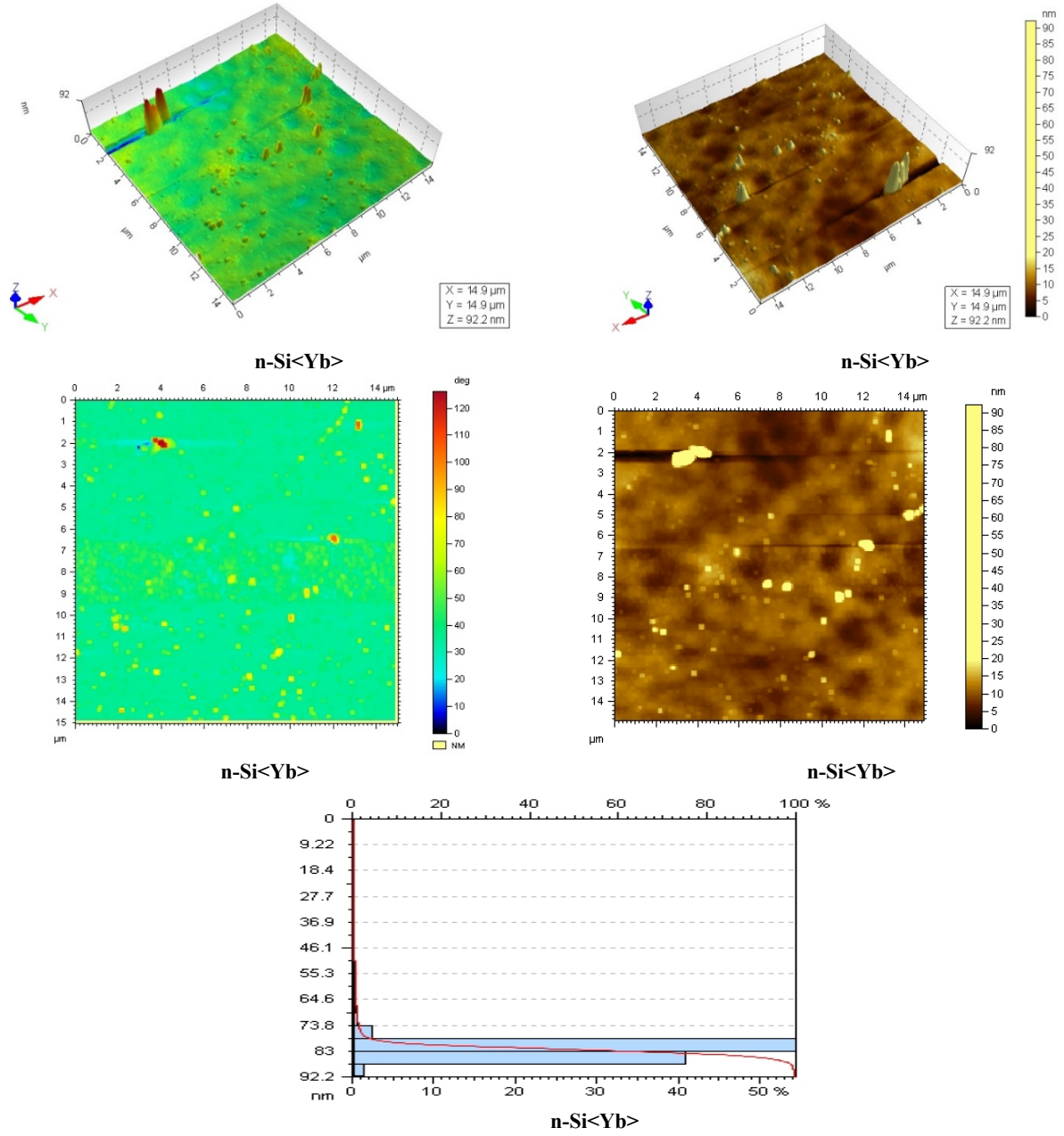

Figure 2. Profile distribution of ytterbium atoms in n-Si doped with ytterbium, obtained by AFM. The image shows the distribution of ytterbium atoms on the surface perpendicular to the sputtered layer

Based on the AFM image presented (Fig. 2), which shows the profile distribution of ytterbium atoms in n-Si doped with ytterbium, an analysis and evaluation of the diffusion coefficient can be conducted. To do this, changes in the structure and surface topography at various depths, as shown in the image, need to be analyzed. The image shows variations in topography and phase contrast, which may indicate the distribution of ytterbium within the silicon. The maximum changes are observed at a depth of approximately 2.36 μm, which can be used as an indicator for the calculation.

To evaluate the diffusion coefficient, we will use Fick's second law for non-stationary diffusion:

$$C(x,t) = \frac{C_o}{\sqrt{4\pi Dt}} exp\left(-\frac{x^2}{4Dt}\right), \quad (3)$$

where:
$C(x,t)$ is the concentration of atoms at depth x at time t,
C_0 is the initial concentration of atoms on the surface,
D is the diffusion coefficient,
t is the diffusion time.

From the image in Fig. 2, it can be assumed that the changes in topography associated with ytterbium diffusion reach a depth of approximately 2.36 μm. The diffusion time t = 15 hours (54,000 seconds), and the depth x = 2.36 μm. The ytterbium concentration at a depth of 2.36 μm is about 10% of the initial surface concentration.

Solving the equation for D:

$$ln\left(\frac{C(x,t)}{C_0}\right) = -\frac{x^2}{4Dt}. \quad (4)$$

Substituting the values:

$$\ln(0{,}1) = \frac{(2.36 \times 10^{-4})^2}{4 \times D \times 54000}$$

$$D = \frac{(2.36 \times 10^{-4})^2}{4 \times 54000 \times ln(10)} \approx 1.9 \times 10^{-15}\ {}^{cm^2}/_{c}$$

The calculated diffusion coefficient of ytterbium in silicon is approximately $\approx 1.9 \times 10^{-15}\ {}^{cm^2}/_{c}$. This value indicates a relatively slow diffusion process, which is typical for rare earth metals such as ytterbium.

Infrared analysis showed that the comparison of the obtained data indicates a significant reduction in the concentration of optically active oxygen N_O^{opt} after ytterbium diffusion (see Fig. 3). Ytterbium doping reduces the concentration of optically active oxygen by 30-40%, depending on the concentration of the added element.

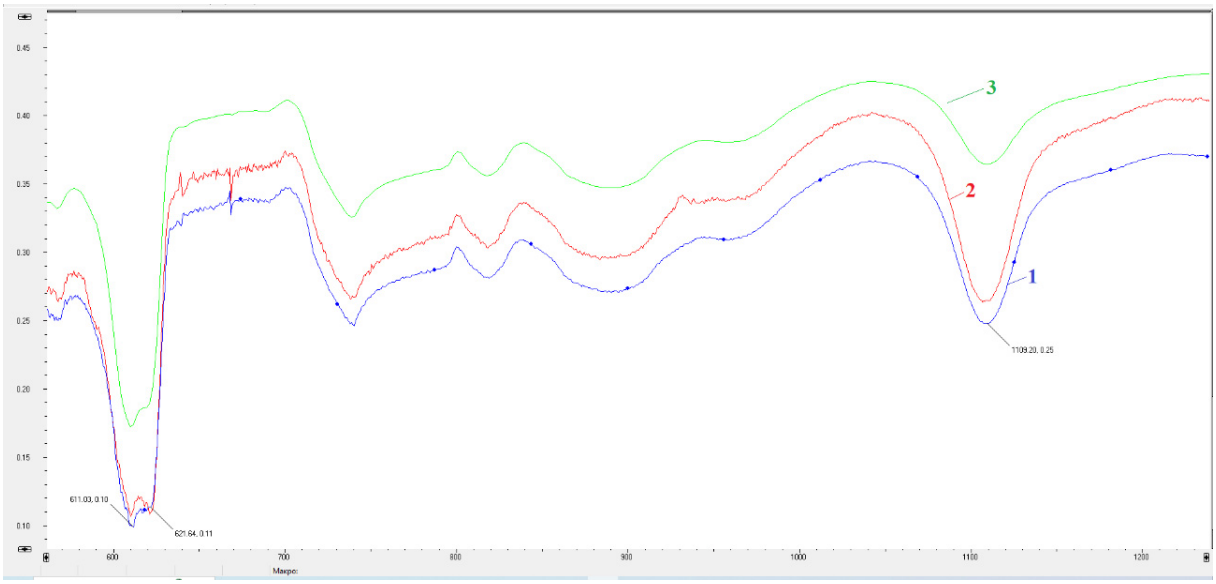

Figure 3. Infrared spectrum of n-type silicon doped with Yb impurities:
1. IR spectrum of control samples (Si_control); 2. IR spectrum of original silicon (Si_original); 3. IR spectrum of n-Si<Yb> samples.

The absorption spectra were recorded in the range from 380 to 7800 cm^{-1}. The concentrations of oxygen and carbon were determined by the intensity of the corresponding peaks in the IR spectra: 1106 cm^{-1} for oxygen and 605 cm^{-1} for carbon. In original silicon, compared to the control sample, an increase in the peak intensity at 1106 cm^{-1} by 5.74% was observed, indicating a slight increase in oxygen concentration. Meanwhile, ytterbium-doped silicon showed a 42.64% reduction in the peak intensity compared to control silicon, indicating a significant decrease in oxygen concentration after doping. Comparing ytterbium-doped silicon with original silicon also revealed a 34.90% reduction in peak intensity, further confirming the decrease in oxygen concentration due to doping. Compared to the control sample, original silicon showed a slight 2.66% increase in peak intensity at 605 cm^{-1}, indicating a small rise in carbon concentration. However, ytterbium-doped silicon demonstrated a 32.45% reduction in the carbon peak intensity, signifying a substantial decrease in carbon concentration after doping. Comparing doped silicon with the original sample also showed a 29.01% decrease in peak intensity, confirming further reduction in carbon concentration due to doping.

Research shows that the capacitance-voltage characteristics of MDS structures based on ytterbium-doped silicon exhibit a shift toward positive bias voltages. This shift is associated with a reduction in surface state density at the Si-SiO_2 interface, indicating changes in the electrical properties of the structure.

The analysis also shows that the effect of ytterbium doping significantly depends on the method of its introduction into the substrate. In the case of diffusion, the capacitance-voltage shift is more pronounced compared to doping during growth, indicating that the diffusion method allows for more efficient penetration of ytterbium into the silicon structure.

Additionally, capacitance-DLTS spectra show the presence of a deep level with an ionization energy of E_c–0.32 eV, whose concentration is determined by diffusion conditions. This result is important for understanding defect formation mechanisms in MOS structures and could serve as a basis for optimizing technological processes in semiconductor device production.

The Raman spectra of the original Si<P> sample are shown in Fig. 4. The spectrum exhibits a high peak in the region of 521 cm^{-1} with a width at half maximum of 8–12 cm^{-1}. The intensity of the first-order scattering at 521 cm^{-1} is due to transverse (TO) and longitudinal (LO) optical phonons. In contrast to the main peak, scattering by second-order acoustic phonons at 303 cm^{-1} (TA) can be observed. Some authors suggest that this peak corresponds to the LA modes [5-18], but there is no exact confirmation of this fact. Probably, we observe a superposition of transverse and longitudinal acoustic modes. There is also a broad peak between 920–1000 cm^{-1}, which is due to the scattering of several transverse optical phonons ~2TO phonons. To date, there is no consensus on the origin of the broad peak. Some authors claim that this peak is formed by a superposition of two or more optical modes [19-23].

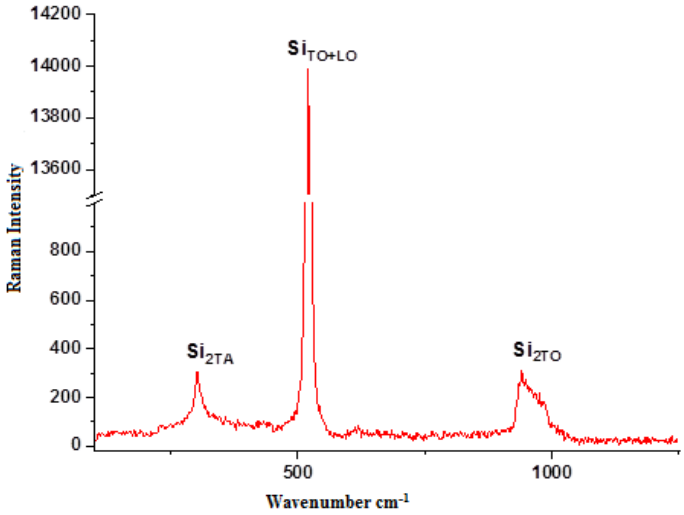

Figure 4. The Raman spectrum of the initial silicon. Oscillatory modes: Si_{2TA} – 303 cm^{-1}, Si_{TO+LO} – 521 cm^{-1}, Si_{2TO} – 920-1000 cm^{-1}

As can be seen from the figure in Fig. 5, further doping of n-Si single crystals with ytterbium impurity atoms leads to some change in the Raman spectra. The results obtained demonstrate that doping silicon with ytterbium leads to significant changes in its structural properties, which is manifested in the form of an increase in the intensity of peaks in the Raman spectra, as well as shifts of these peaks. This graph (Fig. 5) shows the Raman spectra for various ytterbium-doped silicon samples, as well as control samples.

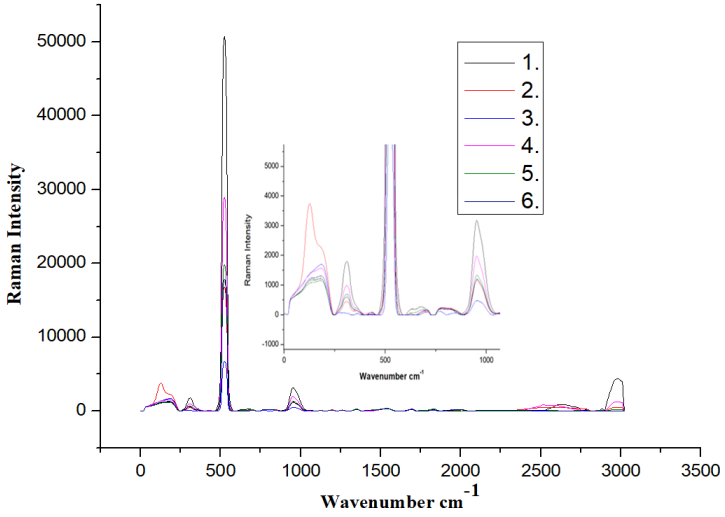

Figure 5. Raman spectra:
1. p-Si original; **2.** p-Si<Yb> (thermal diffusion in the gas phase); **3.** p-Si<Yb> (thermal diffusion in the gas phase), after diffusion 2 μm of the surface were removed; **4.** p-Si<Yb> (Solid-phase thermal diffusion); **5.** p-Si<Yb> (Solid-phase thermal diffusion) after diffusion 2 μm of the surface were removed; **6.** Si control

In ytterbium-doped samples (red line), a significant increase in peak intensity in the range of 200 to 300 cm^{-1} is observed compared to control samples (black line). This may indicate structural changes due to doping, such as an increase in the number of defects or the formation of new phases in the material. It can also be noted that the ytterbium-doped samples exhibit peak shifts compared to control samples. This phenomenon may be related to changes in interatomic distances and internal stresses in the crystal lattice caused by the introduction of ytterbium. The graph shows that different doping or sample treatment methods (e.g., sputtering, diffusion) lead to different peak intensities, indicating differences in the structure and distribution of ytterbium in the silicon matrix.

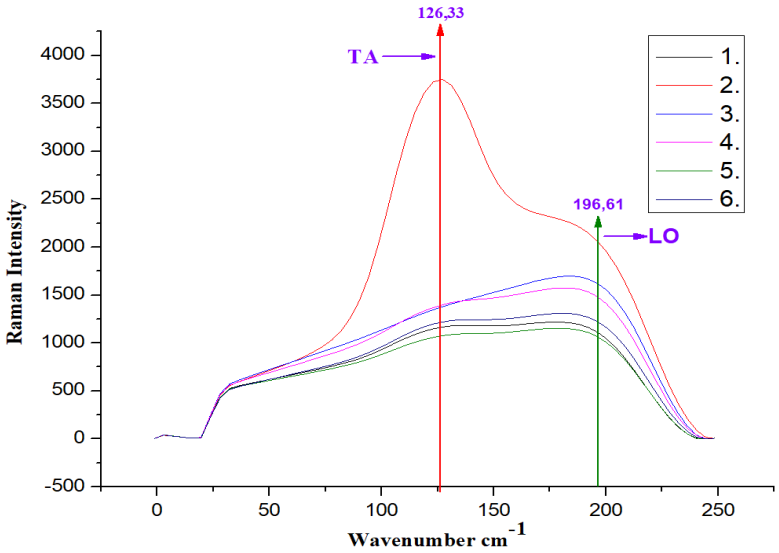

Figure 6. Raman spectrum:

1. p-Si original; **2.** p-Si<Yb> (thermal diffusion in the gas phase); **3.** p-Si<Yb> (thermal diffusion in the gas phase), after diffusion 2 μm of the surface were removed; **4.** p-Si<Yb> (Solid-phase thermal diffusion); **5.** p-Si<Yb> (Solid-phase thermal diffusion) after diffusion 2 μm of the surface were removed; **6.** Si control

The ytterbium-doped samples exhibit a noticeable increase in peak intensity compared to the control sample (Fig. 6). The maximum intensity of the TA peak at 126.33 cm^{-1} significantly surpasses that of similar peaks in the other samples, suggesting a substantial influence of ytterbium on the silicon structure.

The LO peak (196.61 cm^{-1}) also shows an increase in intensity in the ytterbium sputtered sample, indicating possible formation of new phases or enhanced interatomic interactions in the doped samples.

The peak signals of the alloyed samples exhibit a broader shape compared to the control samples (Fig. 7). This suggests a potential increase in defects or stresses within the material's structure following alloying with ytterbium.

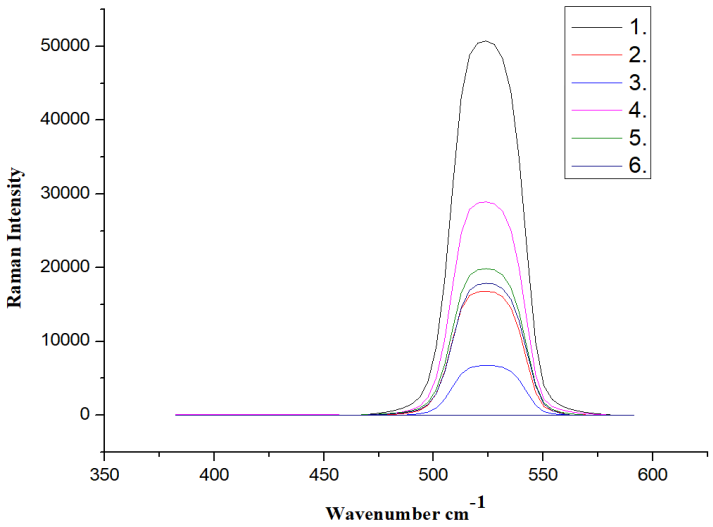

Figure 7. Raman spectrum

1. p-Si original; **2.** p-Si<Yb> (thermal diffusion in the gas phase); **3.** p-Si<Yb> (thermal diffusion in the gas phase), after diffusion 2 μm of the surface were removed; **4.** p-Si<Yb> (Solid-phase thermal diffusion); **5.** p-Si<Yb> (Solid-phase thermal diffusion) after diffusion 2 μm of the surface were removed; **6.** Si control.

A slight shift of the peaks towards shorter wavelengths in the doped samples (Fig. 8) may indicate changes in interatomic distances or the presence of internal stresses within the crystal lattice.

The difference in Raman phonon bands between crystallites and nanocrystallites mainly concerns their bandwidth, while the Raman frequencies are very close, this statement confirms the attribution of the calculated transition to internal stress [24-25].

The Raman spectrum of amorphous layers consists of several broad bands reflecting the single-phonon density of states. When the material is crystalline, the bands narrow and distinct peaks appear. In the case of Si-Yb, three first-order Raman bands associated with Si–Si appear, and vibrations of the Si-Yb and Yb–Yb bonds also appear. The peak position and intensity of these bands depend on the composition, as well as on other factors such as heating, etc., which in turn can contribute to a shift in the frequency of the peaks.

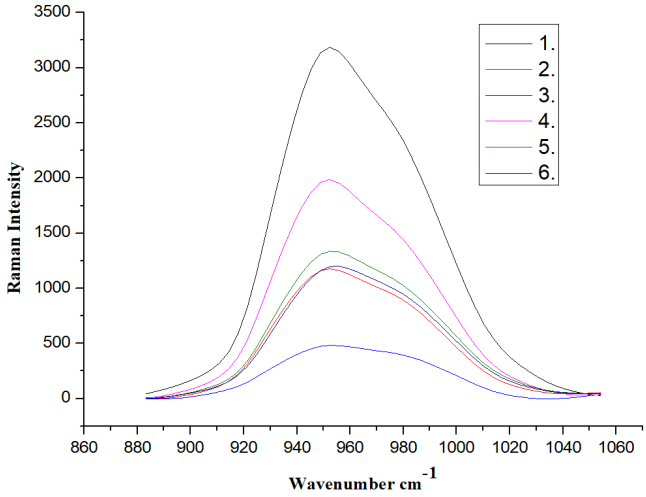

Figure 8. Raman spectrum:

1. p-Si original; **2.** p-Si<Yb> (thermal diffusion in the gas phase); **3.** p-Si<Yb> (thermal diffusion in the gas phase), after diffusion 2 μm of the surface were removed; **4.** p-Si<Yb> (Solid-phase thermal diffusion); **5.** p-Si<Yb> (Solid-phase thermal diffusion) after diffusion 2 μm of the surface were removed; **6.** Si control

The laser beam and temperature induce an ordered state (hereinafter referred to as LTIOS), which is monitored by the Raman spectrum. Further increase in temperature under the influence of light preserves the Raman signature of the nanocrystalline material.

As we have already mentioned, LTIOS appears under light exposure within a certain temperature range for different a-Si-Yb alloy compositions. LTIOS is observed at much lower laser power densities than those required for laser crystallization.

It was found that an increase in the number of defects causes broadening of the amorphous region. A similar relationship should exist for Si-Yb, although, to our knowledge, this has not been previously reported. We noted that the relative intensity of the three Raman scattering bands in Si-Yb systems in the LTIOS state changes. The relative intensity of the Si-Si bond decreases, which in turn indicates that dangling bonds are mainly formed due to Si-Si bond rupture.

CONCLUSIONS

The conducted studies demonstrated that doping silicon with ytterbium leads to significant changes in its structural and physicochemical properties. Observations indicate that doping causes a substantial increase in surface roughness, with the height of irregularities reaching up to 325 nm. This points to a complex microstructure resulting from the uneven distribution of ytterbium atoms, which is also associated with the formation of nanostructures and local stresses in the crystal lattice.

Doping also leads to a marked reduction in the concentration of optically active oxygen by 30-40%, indicating that ytterbium affects the chemical composition and interaction of silicon atoms with oxygen and carbon. The formation of new phases and nanocrystals in the doped samples is accompanied by shifts in the spectra and increased peak intensities, reflecting significant changes in interatomic interactions and the presence of internal stresses in the crystal lattice.

Moreover, the calculated diffusion coefficient of ytterbium in silicon shows a relatively low value, indicating a slow diffusion process typical for rare earth metals. Changes in the electrical characteristics of the material are evident through a reduction in surface state density at the Si-SiO_2 interface and the presence of deep levels with an ionization energy of E_e−0.32 eV.

Overall, the results demonstrate that ytterbium doping has a complex impact on the structure and properties of silicon. This makes the method promising for use in semiconductor electronics and optoelectronics. The obtained data open new opportunities for further research and optimization of technological processes in the development of new semiconductor materials with improved characteristics.

ORCID

Khodjakbar S. Daliev, https://orcid.org/0000-0002-2164-6797; **Sharifa B. Utamuradova**, https://orcid.org/0000-0002-1718-1122
Jonibek J. Khamdamov, https://orcid.org/0000-0003-2728-3832; **Shahriyor B. Norkulov**, https://orcid.org/0000-0002-2171-4884
Mansur B. Bekmuratov, https://orcid.org/0009-0006-3061-1568; **Ulugbek M. Yuldoshev,** https://orcid.org/0009-0003-7575-7497

REFERENCES

[1] L.T. Canham, "Silicon quantum wire array fabrication by electrochemical and chemical dissolution of wafers," Appl. Phys. Lett. **57**, 1046-1990. https://doi.org/10.1063/1.103561
[2] F. Huisken, H. Hofmeister, B. Kohn, M.A. Laguna, and V. Paillard, "Laser production and deposition of light-emitting silicon nanoparticles," Appl. Surf. Sci. **154–155**, 305 (2000). https://doi.org/10.1016/s0169-4332(99)00476-6
[3] V. Vinciguerra, G. Franzo, F. Priolo, F. Iacona, and C. Spinella, "Quantum confinement and recombination dynamics in silicon nanocrystals embedded in Si/SiO_2 superlattices,"J. Appl. Phys. **87**, 8165 (2000). https://doi.org/10.1063/1.373513
[4] F. Koch, and V. Petrova-Koch, "Light from Si-nanoparticle systems - a comprehensive view,"J. Non-Cryst. Solids, **198–200**, 840 (1996). https://doi.org/10.1016/0022-3093(96)00067-1
[5] Zh. Ma, X. Liao, J. He, W. Cheng, G. Yue, Y. Wang, and G. Kong, "Annealing behaviors of photoluminescence from SiO_x:H," J. Appl. Phys. **83**, 7934 (1998). https://doi.org/10.1063/1.367973
[6] M. Zaharias, H. Freistdt, F. Stolze, T.P. Drusedau, M. Rosenbauer, and M. Stutzmann, "Properties of sputtered a-SiO_x:H alloys with a visible luminescence," J. Non-Cryst. Solids, 164–166, 1089 (1993). https://doi.org/10.1016/0022-3093(93)91188-9
[7] U. Kahler, and H. Hofmeister, "Silicon nanocrystallites in buried SiO_x layers via direct wafer bonding," Appl. Phys. Lett. **75**, 641 (1999). https://doi.org/10.1063/1.124467
[8] S. Zhang, W. Zhang, and J. Yuan, "The preparation of photoluminescent Si nanocrystal–SiO_x films by reactive evaporation," Thin Solid Films, **326**, 92 (1998). https://doi.org/10.1016/S0040-6090(98)00532-X
[9] W. Li, G.S. Kaminski Schierle, B. Lei, Y. Liu, and C.F. Kaminski, „Fluorescent Nanoparticles for Super-Resolution Imaging," Chemical Reviews, **122**, 12495−12543 (2022). https://doi.org/10.1021/acs.chemrev.2c00050
[10] A.S. Zakirov, Sh.U. Yuldashev, H.D. Cho, J.C. Lee, T.W. Kang, J.J. Khamdamov, and A.T. Mamadalimov, "Functional Hybrid Materials Derived from Natural Cellulose," Journal of the Korean Physical Society, **60**(10), 1526-1530 (2012). https://doi.org/10.3938/jkps.60.1526
[11] A.S. Zakirov, Sh.U. Yuldashev, H.J. Wang, H.D. Cho, T.W. Kang, J.J. Khamdamov, and A.T. Mamadalimov, "Photoluminescence study of the surface modified and MEH-PPV coated cotton fibers," Journal of Luminescence, **131**(2), 301–305 (2011). https://doi.org/10.1016/j.jlumin.2010.10.019
[12] H. Richter, Z.P. Wang, and L. Ley, "The one phonon Raman spectrum in microcrystalline silicon," Solid State Commun. **39**, 625 (1981). https://doi.org/10.1016/0038-1098(81)90337-9
[13] Z. Iqbal, and S. Veprek, "Raman scattering from hydrogenated microcrystalline and amorphous silicon," J. Phys. C, **15**, 377 (1982). https://doi.org/10.1088/0022-3719/15/2/019
[14] J. Gonzales-Hernandez, G.H. Azarbayejani, R. Tsu, and F.H. Pollak, "Raman, transmission electron microscopy, and conductivity measurements in molecular beam deposited microcrystalline Si and Ge: A comparative study,"Appl. Phys. Lett. **47**, 1350 (1985). https://doi.org/10.1063/1.96277
[15] I.H. Campbell, and P.M. Fauchet, "The effects of microcrystal size and shape on the one phonon Raman spectra of crystalline semiconductors," Solid State Commun. **52**, 739 (1986). https://doi.org/10.1016/0038-1098(86)90513-2
[16] J. Zi, H. Buscher, C. Falter, W. Ludwig, K. Zhang, and X. Xie, "Raman shifts in Si nanocrystals," Appl. Phys. Lett. **69**, 200 (1996). https://doi.org/10.1063/1.117371
[17] D.R. dos Santos, and I.L. Torriany, "Crystallite size determination in μc-Ge films by x-ray diffraction and Raman line profile analysis," Solid State Commun. **85**, 307 (1993). https://doi.org/10.1016/0038-1098(93)90021-E
[18] Kh.S. Daliev, Z.E. Bahronkulov, and J.J. Hamdamov, "Investigation of the Magnetic Properties of Silicon Doped with Rare-Earth Elements," East Eur. J. Phys. **4**, 167 (2023). https://doi.org/10.26565/2312-4334-2023-4-18
[19] Kh.S. Daliev, Sh.B. Utamuradova, Z.E. Bahronkulov, A.Kh. Khaitbaev, and J.J. Hamdamov, "Structure Determination and Defect Analysis n-Si<Lu>, p-Si<Lu> Raman Spectrometer Methods," East Eur. J. Phys. (4), 193 (2023). https://doi.org/10.26565/2312-4334-2023-4-23
[20] P.A. Temple, and C.E. Hathaway, "Multiphonon Raman Spectrum of Silicon," Physical Review B, **7**(8), 3685–3697 (1973). https://doi.org/10.1103/PhysRevB.7.3685
[21] K.J. Kingma, and R.J. Hemley, "Raman spectroscopic study of microcrystalline silica," American Mineralogist, **79**(3-4), 269-273 (1994). https://pubs.geoscienceworld.org/msa/ammin/article-pdf/79/3-4/269/4209223/am79_269.pdf
[22] G.E. Walrafen, Y.C. Chu, and M.S. Hokmabadi, "Raman spectroscopic investigation of irreversibly compacted vitreous silica," The Journal of Chemical Physics, **92**(12), 6987–7002 (1990). https://doi.org/10.1063/1.458239
[23] B. Champagnon, C. Martinet, M. Boudeulle, D. Vouagner, C. Coussa, T. Deschamps, and L. Grosvalet, "High pressure elastic and plastic deformations of silica: in situ diamond anvil cell Raman experiments," Journal of Non-Crystalline Solids, **354**(2-9), 569–573 (2008). https://doi.org/10.1016/j.jnoncrysol.2007.07.079
[24] Sh.B. Utamuradova, H.J. Matchonov, Zh.J. Khamdamov, and H.Yu. Utemuratova, "X-ray diffraction study of the phase state of silicon single crystals doped with manganese," New Materials, Connections Oath Applications, **7**(2), 93-99 (2023). http://jomardpublishing.com/UploadFiles/Files/journals/NMCA/v7n2/Utamuradova_et_al.pdf
[25] Kh.S. Daliev, Sh.B. Utamuradova, J.J. Khamdamov, M.B. Bekmuratov, "Structural Properties of Silicon Doped Rare Earth Elements Ytterbium," East Eur. J. Phys. (1), 375-379 (2024). https://doi.org/10.26565/2312-4334-2024-1-37

ЗМІНИ СТРУКТУРИ ТА ВЛАСТИВОСТЕЙ КРЕМНІЮ ПІД ЧАС ЛЕГУВАННЯ ІТЕРБІЄМ: РЕЗУЛЬТАТИ КОМПЛЕКСНОГО АНАЛІЗУ

Ходжакбар С. Далієв, Шаріфа Б. Утамурадова, Джонібек Дж. Хамдамов, Мансур Б. Бекмуратов, Шахрійор Б. Норкулов, Улугбек М. Юлдошев

Інститут фізики напівпровідників і мікроелектроніки Національного університету Узбекистану, Ташкент, вул. Янгі Алмазара, 20, 100057, Узбекистан

У цій роботі проведено комплексне дослідження структурних, хімічних та електрофізичних властивостей монокристалічного кремнію (Si), легованого ітербієм (Yb). Легування проводили методом термодифузії при температурі 1473 К в умовах високого вакууму з подальшим швидким охолодженням. Для аналізу зразків використовували атомно-силову мікроскопію (АСМ), інфрачервону Фур'є-спектроскопію (FTIR), спектроскопію глибокого рівня (DLTS) і раманівську спектроскопію (RAMAN). АСМ-зображення легованих зразків продемонстрували суттєві зміни рельєфу поверхні. Середньоквадратична шорсткість зросла з менш ніж 10 нм до 60–80 нм, а максимальна висота нерівностей досягла 325 нм. Ці зміни зумовлені утворенням наноструктур внаслідок нерівномірного розподілу атомів ітербію у кристалічній решітці кремнію та виникненням внутрішніх напруг. ІЧ-Фур'є-спектроскопія виявила зниження концентрації оптично активного кисню (N_O^{opt}) на 30-40% після легування, що пов'язано з хімічною взаємодією ітербію з кремнієм. Спектри RAMAN виявили утворення нових фаз та нанокристалів, що свідчить про перебудову кристалічної решітки внаслідок введення ітербію. Коефіцієнт дифузії ітербію в кремнії становить $1{,}9\times10^{-15}$ см²/с, що свідчить про повільний процес дифузії, характерний для рідкоземельних металів. Це також сприяло зниженню густини поверхневих станів на межі Si-SiO_2 і появі глибоких рівнів з енергією іонізації E_c-0,32 еВ.

Ключові слова: *монокристалічний кремній; легування ітербієм; атомно-силова мікроскопія; рамановська спектроскопія; шорсткість поверхні; наноструктури; електричні властивості; MDS-структури; інтерфейс Si-SiO_2*